XAFS study of mixed ligand benzimidazole copper complexes having distorted coordination geometry

V.K. Hinge[a], M. Bairagi[a,b]*, N. Yadav[b], B.D. Shrivastava[b], S.N. Jha[c], D. Bhattacharya[d] and A. Gaur[e]*
[a]Physics Department, Ujjain Engineering College, Ujjain, 456010, India
[b]School of Studies in Physics, Vikram University, Ujjain, 456010, India
[c]Beamline Development and Application Section BARC, Mumbai-400085 and BARC Beamlines Section, RRCAT, Indore, 452013, India
[d]Atomic & Molecular Physics Division, Bhabha Atomic Research Centre, Mumbai, 400085, India
[e]Institute for Chemical Technology and Polymer Chemistry (ITCP), Karlsruhe Institute of Technology, 76131 Karlsruhe, Germany
*monicabairagi14@gmail.com, abhijeet.gaur@kit.edu

Abstract:

X-ray absorption fine structure (XAFS) at the Cu K-edge in copper complexes, viz., $[Cu(BzImH)_4X_2]$, where BzImH= benzimidazole and X= ClO_4 (**1**), NO_3 (**2**), ½ SO_4 (**3**), Br (**4**), Cl (**5**) and their 'inner complex' $[Cu(BzImH)_2]$ (**6**) have been investigated using synchrotron radiation. The crystal structures of **4**, **5** and **6** are not available. From EXAFS analysis, the structures of **4** and **5** have been estimated to be distorted square pyramidal and that of **6** to be tetrahedrally distorted square planar. Though, the crystal structure of the complexes **1** and **2** have been studied earlier using X-ray crystallography and found to be distorted square pyramidal, these complexes have been included in the study because each of these complexes has two independent formula units having two Cu sites in a molecule. In **2** the axial bond lengths are not similar at Cu1 and Cu2 sites. The electronic nature of Cu metal center in the complexes has been studied using XANES. The XANES spectra have been simulated and p-DOS and d-DOS calculated simultaneously for the Cu centre in the complexes. The splitting of Cu K-edge into two edges K_1 and K_2 has been correlated with the p-DOS and the occurrence of pre-edge has been correlated with d-DOS.

Keywords: *Copper complexes, Benzimidazole, Extended X-ray absorption fine structure, X-ray absorption near edge structure, Ab initio calculations, Density of states*

1. Introduction

Benzimidazole and its derivatives are important heterocyclic compounds involved in a variety of biological processes [1]. Their pharmacological, antibacterial, fungicide and anthelmintic activities are well known [2]. Substituted benzimidazoles have attracted great interest especially because it has been reported that the influence of the substitution at the 1, 2 and 5 positions of the benzimidazole ring is very important for their pharmacological effects [3]. Interest in exploring benzimidazole derivatives and their metal complexes has continually increased, since many of these materials may serve as models that mimick both the structure and reactivity of metal ion sites in complex biological systems [4]. Metal coordination polymers based on benzimidazole derivatives are interesting because of their structural diversity and their potential applications in functional materials [5]. Benzimidazole transition metal complexes also exhibit interesting spectral and magnetic properties [4]. Numerous one-, two-, and three-dimensional coordination polymers have been synthesized by the choice of appropriate metal ions and versatile benzimidazole derivatives as ligands [5]. Several studies on transition metal benzimidazole complexes with luminescent properties have been reported [6]. Luminescent metal complexes have potential applications in light emitting devices (LEDs) because of their high luminescence efficiency, high thermal stability and ease of fabrication. Coordination chemistry of benzimidazole and its derivatives with transition metal ions has been reviewed by Téllez et al. [3]. The copper ion is an important metal ion participating in a number of enzymatic processes [2]. The binding of histidine imidazole to copper (II) in various copper proteins has prompted the syntheses and study of copper complexes with potentially chelating ligands incorporating benzimidazole groups [7]. The room-temperature investigation of crystal and molecular structure of dibromobis(benzimidazole)copper(II) has been carried out by Bukowska-Strzylewska and Tosik, [8]. Haddad and Hendrickson [9] have prepared $[Cu_2(tren)_2(BzIm)](ClO_4)_3$ where tren is 2,2',2''-triaminotriethylamine and studied its EPR and magnetic susceptibility.

In the present investigation, X-ray absorption spectroscopy (XAS) at the Cu K-edge has been used to study the local and electronic structure of the copper complexes involving benzimidazole (BzImH) and other inorganic anionic ligand (X), viz: $[Cu(BzImH)_4X_2]$, where X= ClO_4 (**1**), NO_3 (**2**), ½ SO_4 (**3**), Br (**4**), Cl (**5**), and their inner complex $[Cu(BzImH)_2]$ (**6**). The crystal structures of **4** and **5** are not available. Their EXAFS has been analyzed to obtain information about their coordination geometry. Though, the crystal

structure of the complexes **1** and **2** have been studied earlier using X-ray crystallography [2, 10] and found to be distorted square pyramidal, these complexes have been included in the study because each of these complexes has two independent formula units having two Cu sites Cu1 and Cu2 in a molecule. In **1,** the Cu1 and Cu2 sites have similar axial bond lengths 2.467-2.465 Å, but in **2** the axial bond lengths are not similar, the bond lengths being 2.59 Å at Cu1 site and 2.47 Å at Cu2 site. EXAFS analysis of these complexes has been done to probe if similar information about the two independent formula units can be obtained about the two Cu sites. Complex **3** does not have two independent formula units. Its EXAFS has been analyzed using its own available crystallographic data [1]. A review of the earlier studies [11-15] shows that the structure of complex $Cu(BzImH)_2$ (**6**) is uncertain, there being conflicting reports about the structure of the complex, which has not been studied by X-ray crystallography. Goodgame and Haines [11] have assigned it distorted tetrahedral structure. Cordes and Walter [12] have suggested that the configuration of the complex is probably planar. In a detailed review article of Sundberg and Martin [13], the structure of the complex is reported to be uncertain as it probably contains at least some of its Cu(II) ions in a tetrahedral environment. Drolet et al. [14] have proposed a structure of the complex in which Cu is shown to be coordinated by four N atoms, but no geometry was proposed. Hence, we have investigated the local structure around Cu atom in $Cu(BzImH)_2$ (**6**) by XAS. The complete list of complexes studied and mentioned in the present work, with their codes and molecular formula are given in Supplementary Information section S1.

In the present study, the electronic nature of Cu metal center has also been studied using XANES in the six complexes **1-6**. The XANES spectra have been simulated for the Cu centre in the complexes using software *FEFF10* and compared with the experimental XANES spectra. Further, p-DOS and d-DOS calculated simultaneously for absorbing Cu metal center have been correlated with the features and shape of the simulated XANES spectra as well as of the experimental spectra. A reason for undertaking the present investigation was also that in the earlier investigations [16-18] on these complexes, the EXAFS was not analyzed by fitting theoretical model and XANES was not analyzed by simulating the spectra and calculating p-DOS.

2. Experimental

The complexes **1-6** have been prepared and characterized by following methods described by Goodgame and Haines [11]. The X-ray absorption spectra (XAS) of the

complexes have been recorded at the K-edge of copper on BL-9 scanning type EXAFS beamline at 2.5 GeV Indus-2 synchrotron source at Raja Ramanna Centre for Advanced Technology (RRCAT), Indore, India [19]. The main constituent of this beamline is a Double Crystal Monochromator (DCM), which has two Si (111) crystals carved out in a single block, the second crystal being sagittal cylinder. The spectrum of Cu metal foil was simultaneously recorded for the purpose of energy calibration. For calibration purpose, the first inflection point in the derivative spectrum of Cu metal foil was assigned the value of ~8979 eV. For recording XAS of the Cu complexes, absorption screens were prepared in the form of pellets from the calculated amount of sample, mixed with a cellulose (binder). EXAFS data analysis was performed using the software packages *Athena* and *Artemis* [20], the details of which are given in SI section S2.

3. Results and discussions:

3.1. EXAFS analysis

3.1.1 Complexes 1 and 2: In order to investigate whether EXAFS can yield information about the two independent formula units in the same complex, the experimental data of complexes **1** and **2** have been analysed as follows. In the crystallographic data (CIF) of Dobrzynska et al (2010) [2] for complex **1** and Zhou et al (2011) [10] for complex **2**, which have been used to generate theoretical models, the copper atom has been labeled as Cu1 in one formula unit and as Cu2 in another formula unit. Hence, two theoretical models have been generated by firstly putting in *Artemis* Cu1 as core atom and then secondly Cu2 as core atom. By fitting the two theoretical models, one by one, with the experimental spectra of the complexes, we have obtained the local structure parameters around Cu1 and Cu2 atoms in each of the two complexes. The theoretically fitted spectra in R-space for Cu1 and Cu2 sites are shown in figs. 1(a and b) for complex **1** and in figs. 1(c and d) for complex **2.** The contributions of the different paths used in the fitting are also given in these figures. The experimental k^3 weighted $\chi(k)$ vs. k spectra along with theoretically fitted spectra are given in figs. S1(a and b) for complex **1** and figs. S2(a and b) for complex **2**. The results are given in tables 1(a) and (b) for complexes **1** and **2** respectively. The results obtained from EXAFS agree well with those obtained from crystallography for the four N atoms forming the square base as well as the O atom at apical position, in both the independent formula units. In complex **1**, the distances of O atom at apical position, i.e., Cu1-O and Cu2-O have been

found to be same, i.e., 2.47 Å, while the values reported from crystallography [2] are 2.467 Å and 2.465 Å. In complex **2**, the distance of O atom at apical position have been found to be, i.e., Cu1-O = 2.55 Å and Cu2-O = 2.45 Å, while the values reported from crystallography [10] are 2.589 Å and 2.468 Å. Thus, the values of the distance of O atom at apical position from the absorbing Cu atom are found to be different in the two-formula units in complex **2**, as also observed from single crystal structure study. Thus, it has been shown that EXAFS can yield information about the two independent formula units in the same complex. The geometry of complexes around the two Cu sites Cu1 and Cu2 are given in figs. 3(a and b) for complex **1** and 3(c and d) for complex **2**. Hence, it can be inferred that in case of a sample containing two formula units in a molecule, information about the two formula units can be obtained separately and satisfactorily from the analysis of EXAFS.

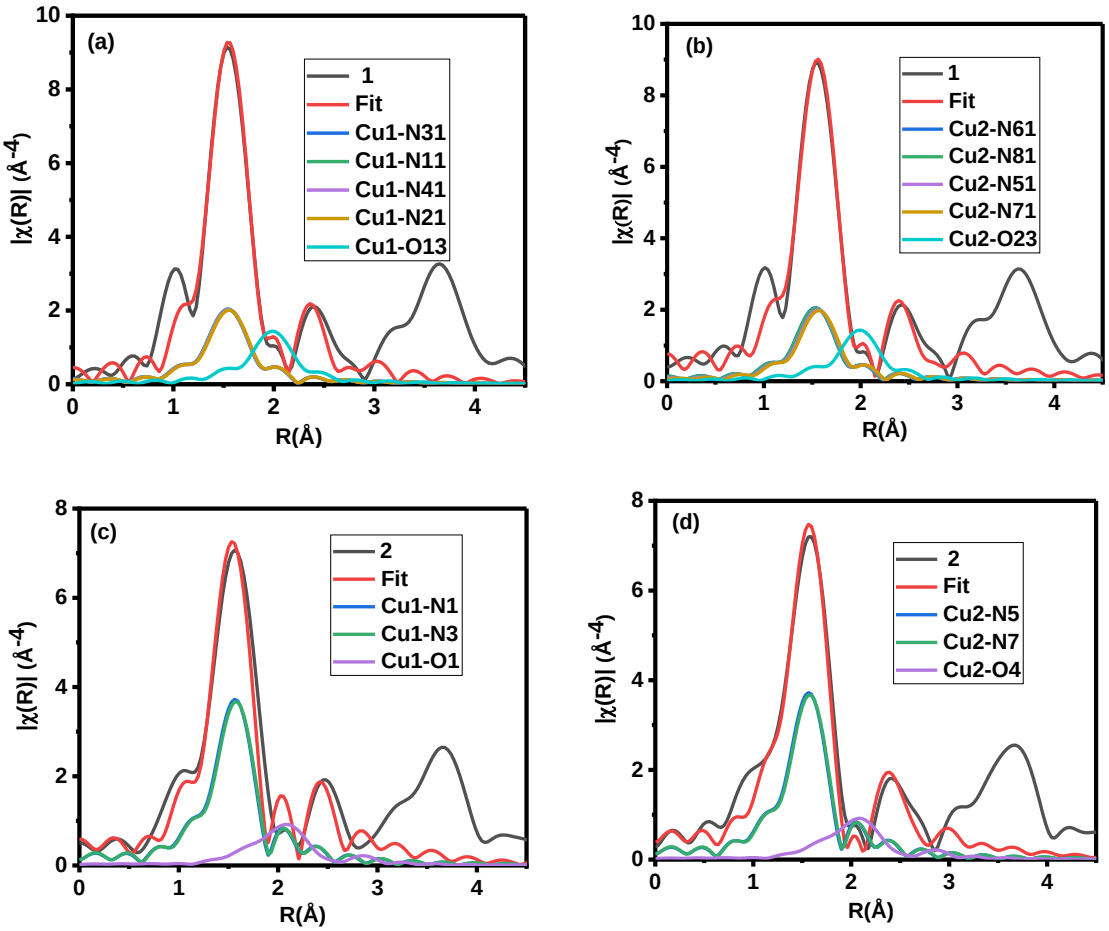

Fig.1 EXAFS fitting for complexes **1** (a) Cu1 site and (b) Cu2 site and **2** (c) Cu1 site and (d) Cu2 site in R-space along with contributions of the different paths, showing the experimental curve (black line) and the theoretical fit (red line) with the theoretical models generated using their own crystallographic data.

3.1.2 Complex 3: The crystal structure of complex **3** has been studied by Sieron [1] and is found to be square pyramidal. It does not have two formula units like that discussed above

in complexes **1** and **2**. The crystallographic data of Sieron [1] for complex **3** has been used as input in *Artemis* to generate the theoretical model, which has been fitted to its experimental data. The theoretically fitted spectra in R-space along with contributions of the different paths used in the fitting are shown in fig 2(a). The experimental k^3 weighted $\chi(k)$ vs. k spectra along with theoretically fitted spectra are given in fig. S3(a). The local structure parameters around the absorbing Cu atom obtained as a result of the fitting are given in table 1(b). It can be seen that the bond distances obtained from EXAFS agree well with those reported by crystallography [1] (also given in the table) and reveal the geometry of the complex as square pyramidal. The four N atoms form the square base with Cu atom at the center, the Cu-N distances being in the range from 1.98-2.01 Å. The O atom is at the top of pyramid at a distance of 2.19 Å from the Cu atom. The apical bond length Cu-O in complex **3** is found to be shorter in comparison to that in complexes **1** and **2**. The geometry of complex around the Cu atom is given in fig. 3(e).

3.1.3 Complexes 4 and 5: The crystal structures for complexes **4** and **5** are not available but their molecular structure is analogous to the three complexes **1-3** studied in the present work. For analyzing the EXAFS of **4** and **5**, we have generated the theoretical model for the Cu1 site of complex **1** after replacing the axial O atom by Br/Cl atom and then fitted it to the experimental data of complexes **4** and **5**. The theoretically fitted spectra in R-space are shown in fig. 2(b) for complex **4** and in fig. 2(c) for complex **5.** The contributions of the different paths used in the fitting are also given in these figures. The experimental k^3 weighted $\chi(k)$ vs. k spectra along with theoretically fitted spectra are given in fig. S3(b) for complex **4** and fig. S3(c) for complex **5**. The results are given in table 1 (b) for complexes **4** and **5** respectively. The geometry around Cu atom has been estimated to be square pyramidal with the four N atoms forming the square base with Cu at center, the Cu-N distances being in the range from 1.99-2.00 Å and the O atom at the top of pyramid at a distance of 2.46 Å and 2.44 Å from the Cu atom in complexes **4** and **5**, respectively. The apical bond lengths Cu-O in complexes **4** and **5** are found to be of the same order as those obtained for both the sites Cu1 and Cu2 in complex **1** and for site Cu2 in complex **2**, but shorter in comparison to that for site Cu1 in complex **2.** The geometry of complexes **4** and **5** around the Cu atom is shown in figs. 3 (f and g).

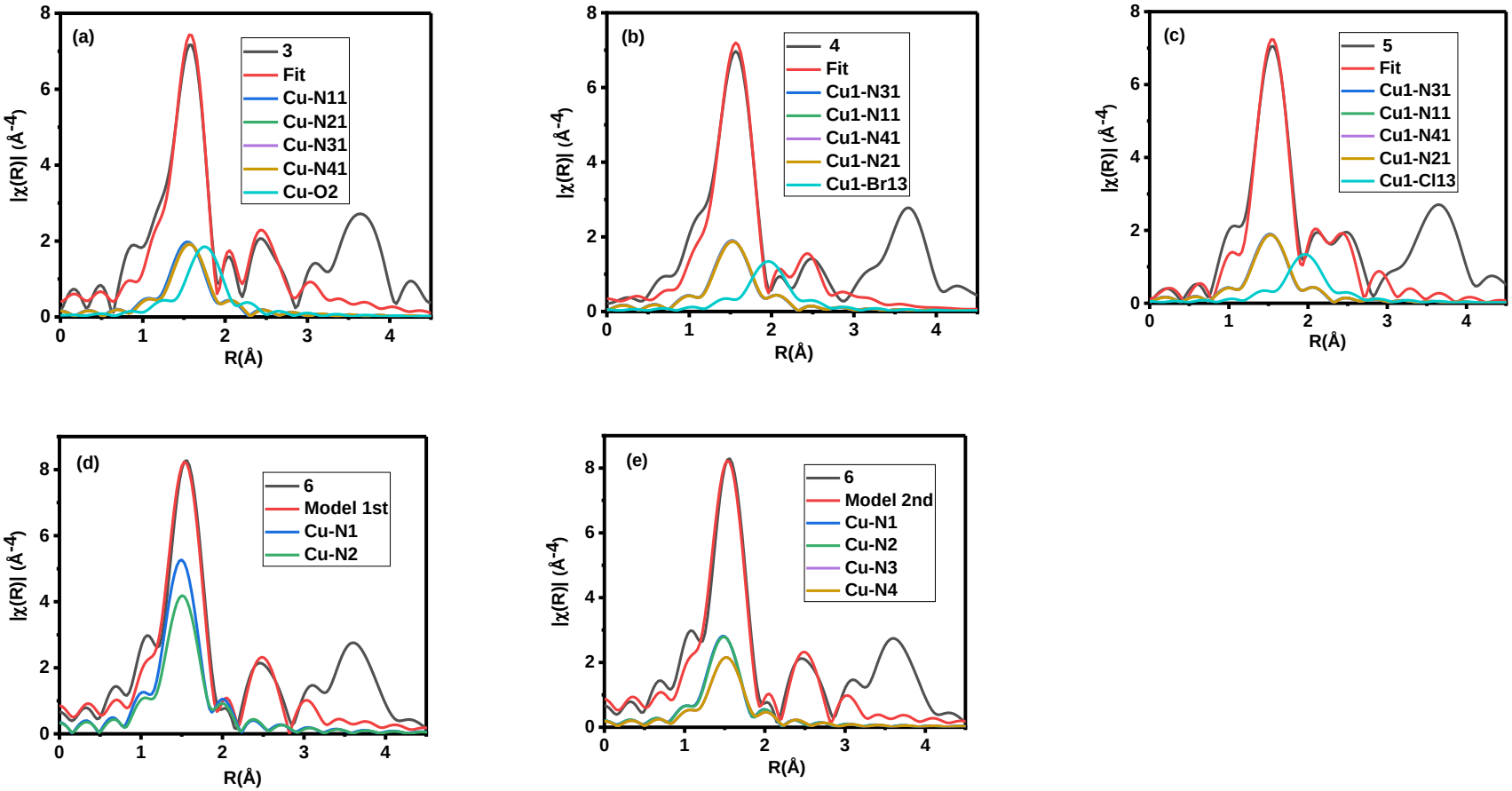

Fig 2 EXAFS fitting in R-space along with contributions of the different paths, showing the experimental curve (black line) and the theoretical fit (red line) for complexes (a) **3** using its own crystallographic data, (b) **4** using crystallographic data of complex **1** (Cu1 site), (c) **5** using crystallographic data of complex **1** (Cu1 site), (d) **6** using square planar model and (e) **6** using tetrahedrally distorted square planar model

Table 1 Structural parameters obtained from EXAFS fitting for the complexes. N=coordination no., R=Bond distance, R_c= crystallographic value, σ^2= Debye-Waller factor. '*R factor*'= Goodness of fit parameter. The error bars are given in parenthesis.

Table 1(a): Complex 1: $[Cu(BzImH)_4](ClO_4)_2$									
Absorbing site Cu1					**Absorbing site Cu2**				
S_0^2 =1.09, ΔE=7.6(1.5) eV, '*R factor*'=0.000645					S_0^2 =1.08, ΔE=6.9(0.8) eV, '*R factor*'=0.004096				
Atomic pairs	N	R (Å)	σ^2 x10^3 (Å^2)	R_c (Å) [2]	Atomic pairs	N	R (Å)	σ^2 x10^3 (Å^2)	R_c (Å) [2]
N31	1	1.98(0.01)	3.7(1.2)	1.994	N61	1	1.96(0.01)	3.4(1.1)	1.977
N11	1	1.98(0.01)	3.7 (1.2)	1.995	N81	1	1.97(0.01)	3.4 (1.1)	1.980
N41	1	1.98(0.01)	3.7 (1.2)	1.998	N51	1	1.99(0.01)	3.4 (1.1)	2.001
N21	1	1.99(0.01)	3.7 (1.2)	2.005	N71	1	1.99(0.01)	3.4 (1.1)	2.013
O13	1	2.47(0.03)	7.6 (4.5)	2.467	O23	1	2.47(0.02)	9.5 (3.2)	2.465
Complex 2: $[Cu(BzImH)_4](NO_3)_2$									
S_0^2=0.95, ΔE=10.2(1.2) eV, '*R factor*'=0.009919					S_0^2=1.09, ΔE=8.4(1.2) eV, '*R factor*'=0.004163				
Atomic pairs	N	R (Å)	σ^2 x10^3 (Å^2)	R_c (Å) [10]	Atomic pairs	N	R (Å)	σ^2 x10^3 (Å^2)	R_c (Å) [10]
N1	2	1.97 (0.01)	4.3 (1.5)	1.997	N5	2	1.98(0.01)	5.3(1.1)	1.989
N3	2	1.98 (0.01)	4.3 (1.5)	2.008	N7	2	1.99(0.01)	5.3(1.1)	1.993
O1	1	2.55 (0.03)	6.7 (4.7)	2.589	O4	1	2.45(0.01)	10.4 (2.9)	2.468

Table 1(b)								
		Complex 3: $[Cu(BzImH)_4]SO_4$			**Complex 4: $[Cu(BzImH)_4]Br_2$**		**Complex 5: $[Cu(BzImH)_4]Cl_2$**	
		S_0^2=1.10, ΔE=8.6(1.0) eV, '*R factor*'=0.000585			S_0^2=1.07, ΔE=6.6(1.1) eV, '*R factor*'=0.007016		S_0^2 =1.00, ΔE=8.0(1.3) eV, '*R factor*' =0.017358	
Atomic pairs	N	R (Å)	σ^2 x10^3 (Å^2)	R_c(Å) [1]	R (Å)	σ^2 x10^3 (Å^2)	R (Å)	σ^2 x10^3 (Å^2)
N31	1	2.01(0.01)	5.3(0.9)	2.018	1.99(0.01)	5.5(1.6)	1.99(0.01)	4.8(2.6)
N11	1	1.98(0.01)	5.3(0.9)	1.995	1.99(0.01)	5.5(1.6)	1.99(0.01)	4.8(2.6)
N41	1	2.01(0.01)	5.3(0.9)	2.023	2.00(0.01)	5.5(1.6)	2.00(0.01)	4.8(2.6)
N21	1	2.00(0.01)	5.3(0.9)	2.013	2.00(0.01)	5.5(1.6)	2.00(0.01)	4.8(2.6)
O2/Br/Cl	1	2.19(0.02)	17.6 (14.1)	2.205	2.46(0.05)	22.7(7.5)	2.44(0.02)	11.0(5.8)

Table 1(c) Complex 6: $Cu(BzImH)_2$						
	Square planar model [21]			**Distorted square planar model** [22]		
	S_0^2=1.02, ΔE=9.3(0.7) eV, R factor=0.003145, χ_ν^2= 202			S_0^2=1.02, ΔE=7.2(1.2) eV, R factor=0.003005, χ_ν^2= 187		
Atomic pairs	N	R (Å)	σ^2 x10^3 (Å^2)	N	R (Å)	σ^2 x10^3 (Å^2)
N1	2	1.94(0.01)	5.0 (1.0)	1	1.93(0.01)	4.8 (1.0)
N2	2	1.97(0.01)	5.0 (1.0)	1	1.94(0.01)	4.8 (1.0)
N3				1	1.99(0.01)	4.8 (1.0)
N4				1	1.99(0.01)	4.8 (1.0)

3.1.4 Complex 6: As already pointed out in the introduction, that there are conflicting reports about the structure of complex **6**, which has not been studied by X-ray crystallography. As mentioned in the Introduction section, a review of the earlier studies shows that the structure of Cu(II) complex $Cu(BzImH)_2$ is uncertain. Hence, in the present study, we have tried to find the local structure around Cu atom in $Cu(BzIm)_2$ (**6**) by

analyzing its EXAFS using three different theoretical models, each having Cu(II) as absorbing atom surrounded by four N/O atoms. The first model used is for square planar geometry. The CIF file used for generating the model is for the Cu(II) complex Bis[2-(1H-benzimidazol-2-yl)benzoato] copper(II) dihydrate $[Cu(C_{14}H_9N_2O_2)_2]$ $2H_2O$ (**7**) [21]. The second model used is for tetrahedrally distorted square planar geometry. The CIF file used for generating the model is for $[Cu_2(L_1)_2]$.EtOH (**8**) (where L_1=m-xylenediamine) [22]. The third model used is for tetrahedral geometry. The CIF file used for generating the model is for the Cu(II) complex $Cu(OOC(CH_3)_2C_6H_5)(HB(3,5\text{-}iPr_2pz)_3$ (where $HB(3,5\text{-}iPr_2pz)_3$=hydrotris(3,5-diisoropyl-1-pyrazolyl)borate [23].

The fitting of these three theoretical models to the experimental data of complex **6** has been done by following the procedure as mentioned in SI section S2. The values of ranges for k, R and k_w have been kept exactly the same in the three fittings. Four carbon paths have also been included in the fitting. The third fitting could not be done satisfactorily, as the values of S_0^2 and σ^2 were not proper. Hence, the results for this fitting are not given here. The results obtained from the first and second fittings are given in table 1(c). The fittings in k-space and R-space for the first theoretical model are shown in figs. S4(a) and 2(d) respectively. Similarly, the fittings in k-space and R-space for the second theoretical model are shown in figs. S4(b) and 2(e) respectively. To compare the first and second fittings, we have relied on the values of χ_ν^2. The value of χ_ν^2 for the square planer model is 202 and for tetrahedrally distorted square planar model is 187. On this basis, we suggest that the structure of complex **6** is closer to the tetrahedrally distorted square planar around the central Cu atom with the four N atoms having Cu atom at the center, the Cu-N distances being in the range from 1.93-1.99 Å. The geometry of complex around the Cu atom is shown in fig. 3(h).

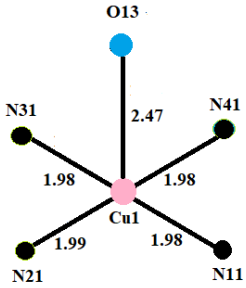

(a) Complex **1** (Cu1 site)

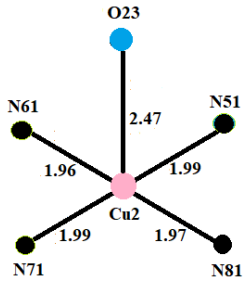

(b) Complex **1** (Cu2 site)

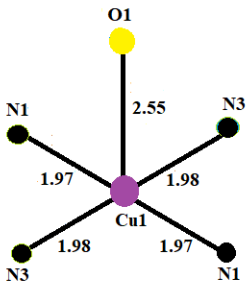

(c) Complex **2** (Cu1 site)

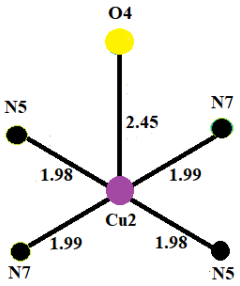

(d) Complex **2** (Cu2 site)

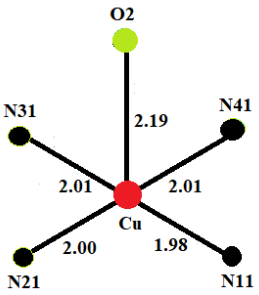

(e) Complex **3**

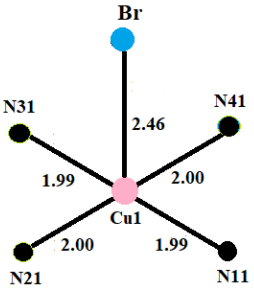

(f) Complex **4**

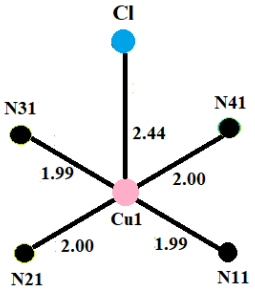

(g) Complex **5**

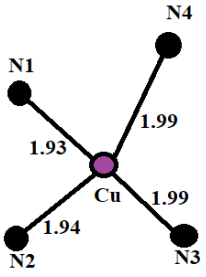

(h) Complex **6**

Fig.3 Square pyramidal coordination geometry for Cu in complex **1** at (a) Cu1 site and (b) Cu2 site, in complex **2** at (c) Cu1 site and (d) Cu2 site, in complex **3** (e), complex **4** (f) complex **5** (g). Tetrahedrally distorted square planar geometry of complex **6** (h). The bond lengths shown (in Å) are determined from EXAFS analysis.

3.2. XANES interpretation:

Normalized Cu K-edge XANES spectra for the complexes **1-6** are shown in Fig. 4(a). The K-edge is seen split into two portions: K_1 and K_2. The pre-edge peak, marked as P, is very weak. The white line W has been found to have broadened structure between the two arrows marked in the figure. The reference spectra of Cu metal, CuO, Cu_2O and

$Cu(CH_3COO)_2$ showing characteristic XANES features for different oxidation states and coordination geometries of Cu are given in fig. 4(b) for comparison.

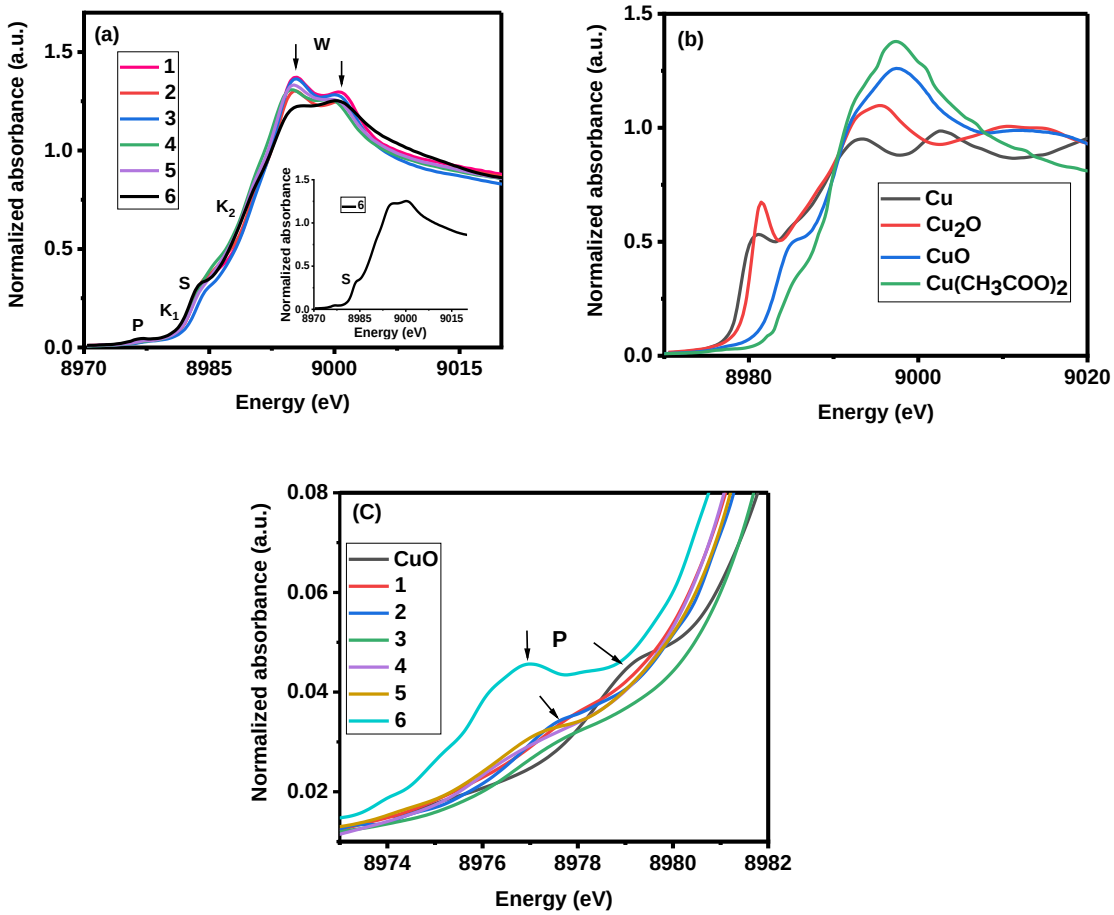

Fig.4 (a)Normalized Cu K-edge XANES spectra for the complexes **1-6.** Inset shows the shoulder S in complex **6**. (b) The spectra of Cu metal, CuO, Cu_2O and $Cu(CH_3COO)_2$ are also included for comparison. The pre-edge peak is marked as P. White line is marked as W and has a broadened structure between the two arrows. The K-edge is seen split into two portions: K_1 and K_2. (c) Pre-edge peak P, shown enlarged, in the Cu K-edge XANES spectra of complexes **1-6**.

The characteristic XANES features observed in the complexes are indicative of the different geometries. One of such features is the shoulder in the rising part of the Cu K-absorption edge. The shoulder is prominent in CuO (square planar geometry) and diminished in $Cu(CH_3COO)_2$ (square pyramidal geometry) [24]. In the presently studied complexes, while in complex **6**, the shoulder is clearly visible, in complexes **1-5**, the shoulder is diminished showing that the coordination geometry of complex **6** (tetragonally distorted square planar) is different than those of complexes **1-5** (square pyramidal). The observed characteristic XANES features in the complexes are further discussed as follows.

3.2.1. Chemical shift – The derivative spectra of the XANES region is shown in Fig. 5. From this figure, the energy of the Cu K-edge in the complexes has been determined from the first peak in the derivative XANES spectra, because this peak corresponds to the inflection point of the K_1 portion of the edge. The shift in the edge energy of the complexes with respect to that of Cu metal (8979 eV), known as chemical shift, is found to be 4.1, 4.3, 4.5, 4.2, 3.9, 3.9 eV for complexes **1**-**6** respectively (table 2). Thus, the Cu K-edge in the complexes is found to be shifted to the higher energy as compared to that of Cu metal. In the standard compounds Cu_2O and CuO, the shift is found to be 1.2 eV and 5.9 eV respectively. On comparing these shifts with those obtained for the complexes **1**-**6**, it can be seen that the complexes **1**-**6** show shifts of the order of that obtained in CuO. Since, the chemical shift is a good indicator of the oxidation state of the absorbing atom, it can be concluded that Cu is in +2 oxidation state in the complexes **1**-**6**.

3.2.2. Pre-edge peak - A pre-edge peak P has been found just before the Cu K-edge in the complexes **1**-**6**. It is seen with difficulty in the XANES spectra (fig. 4(a)). However, it is seen clearly in fig. 4(c), which is a blown-up figure of the lower energy portion of fig. 4(a). In the reference spectra, this peak is observed in CuO and not in Cu_2O as it is attributed to the 1s→3d quadrupole transition having low intensity and may occur in square-pyramidal geometry [25-28]. The pre-edge peak has been analyzed using the module available in software *Larch* [29]. Firstly, the background has been subtracted from the experimental data and then the separated peak has been fitted by Pseudo-Voigt function. The procedure has been shown in SI section S3 in figs. S5(a)-(f) for complexes **1**-**6** respectively. The values of centroid, height, and area (amplitude) of pre-edge peak are given in table 3 and in figs. S5(a)-(f). In all the complexes, the centroid of the peak is observed at energy between 8977.1 to 8977.8 eV. The centroid in the case of complex **6** is at 8976.7 eV and has maximum intensity among the six complexes. The pre-edge features have been correlated with d-density of states in section 3.3.2.

3.2.3. White line – In the XANES spectra of the complexes **1**-**6** (fig. 4(a)), the white line, marked as W, has a broadened structure consisting of two peaks marked by two arrows in the figure. The separation of the peaks is 5.7-5.9 eV in complexes **1**-**5** and 5.0 eV in complex **6**. The white line is assigned to the transitions from Cu 1s orbital to molecular orbitals, mainly the 4p orbitals [27]. Generally, the intensity of white line decreases with decreasing

coordination number [24]. In fig. 4(a), while the intensity of white line of the complexes **1-5** is observed to be nearly the same, the intensity of the complex **6** is found to be less. The decrease in intensity from complexes **1-5** to complex **6** is in accordance with the decrease in coordination number, since the coordination number of complexes **1-5** is five and that of complex **6** is four. Further discussion regarding the two-peak feature of white line is given in section 3.3.3.

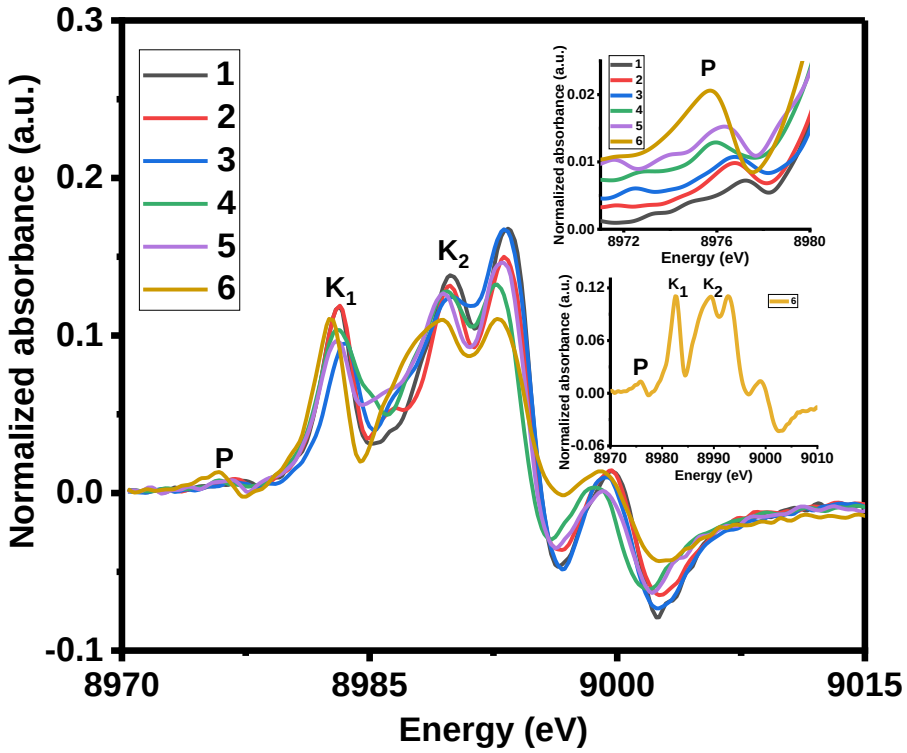

Fig.5 Derivative XANES spectra of complexes **1**-**6**. Energies of the peaks K_1 and K_2 give the energies of the inflection points of the two portions K_1 and K_2 of the K-edge respectively. Energy of K_1 is taken as the energy of the Cu K-edge of the complex. Upper inset shows the pre-edge peak P in the normalized μ(E) spectra of the complexes. Lower inset shows the derivative μ(E) spectrum of complex **6**.

3.2.4. Derivative spectra – In the XANES spectra of complexes (fig. 4(a)), the main Cu K absorption edge, i.e., the rising part in the absorption spectra is found to be split into two edges K_1 and K_2 by a weak shoulder. The splitting of the edge is seen distinctly in the derivative spectra of the complexes (fig. 5) in the form of two separate peaks K_1 and K_2. The derivative spectra clearly indicate that a weak shoulder like structure indeed exists on the low-energy side of the edge.

In fig. 5, it is observed that the two peaks K_1 and K_2 nearly overlap each other in the complexes **1-5** since their positions are nearly the same. There is difference in intensities of the two peaks and this difference is also nearly the same in these complexes. Their similar nature shows that complexes **1-5** have similar coordination (square pyramidal) around Cu

center. In complex **6**, there is hardly any difference in the intensities of two peaks, indicating that complex **6** have difference coordination (tetrahedrally distorted square planar).

The separation between the two edges K_1 and K_2 has been determined from the difference of energies of the two peaks K_1 and K_2 in the derivative spectra and is given in table 2. The K-edge is due to electric dipole-allowed 1s→4p transition and the split portions K_1 and K_2 are due to $1s \rightarrow 4p_{xy}$ and $1s \rightarrow 4p_z$ transitions respectively. While, the feature K_1 has been reported to reflect the distortion in the Cu cluster, the feature K_2 is said to reflect the axial geometry of the metal clusters [25]. Further, the energy separation between the peaks K_1 and K_2 is expected to give an estimate of the destabilization of the $4p_z$ metal orbital. Since the $4p_z$ destabilization can be correlated to the axial (z axis) bond length, hence the separation between peaks K_1 and K_2 should depend on the axial bond length.

Table 2 XANES experimental data and analysis data

	Experimental data				Determined from EXAFS analysis	Theoretical p-DOS data
Complex	E_{K1} (eV)	E_{K2} (eV)	Chemi-cal shift* (eV)	Separation (E_{K2}-E_{K1}) (eV)	Axial bond length (Å)	Separation of two peaks K_1 and K_2 (eV)
1	8983.1	8989.8	4.1	6.7	2.47 (for Cu1), 2.47 (for Cu2)	7
2	8983.3	8989.8	4.3	6.5	2.53 (for Cu1), 2.45 (for Cu2)	6.5
3	8983.5	8989.6	4.5	6.1	2.19	6.3
4	8983.2	8989.8	4.2	6.6	2.46	7
5	8982.9	8989.4	3.9	6.5	2.44	7
6	8982.9	8989.0	3.9	6.1	-	5

Note: *Chemical shift= E_{K1}(Compound)-E_{K1}(Cu metal)
E_{k1}(Cu metal) = 8979 eV
Chemical shifts for Cu_2O and CuO are respectively 1.2eV and 5.9eV

Table 3 Pre-edge peak experimental data and analysis data

	Experimental data of pre-edge peak					Theoretical d-DOS data		
Com plex	E(Centr-oid) (eV)	E(com-plex)*-E(cent-roid)	Height (arb. units) $\times 10^{-3}$	Area (arb. units) $\times 10^{-3}$	χ_ν^2 ** $\times 10^{-8}$	Position of maxima (eV)	Height of maxima (arb. units)	Area of curve (arb. units)
1	8977.8	10.4	9.2	58	3.7	10.4	4.4	10.8
2	8977.6	10.6	6.2	14	3.0	10.4	2.7	10.4
3	8977.6	10.6	4.4	11	3.7	11	2.6	9.6
4	8977.1	10.4	6.4	27	2.5	10.4	4.4	10.8
5	8977.1	10.4	6.3	21	8.3	10.4	4.4	10.8
6	8976.7	10.7	13	35	2.1	15	10	8.6

Note: *E(complex) has been determined as a energy corresponding to normalized μx=0.5 [30,31]
**χ_ν^2 is the parameter for fitting the Pseudo-Voigt function to the pre-edge peak

In complexes **1** and **2** there are two independent centers Cu1 and Cu2. While in complex **1** the axial distance is same (2.47 Å) for both of the centers, in complex 2 the axial distances are different: Cu1-O=2.55 Å and Cu2-O=2.45 Å. In the remaining three complexes **3**, **4**, and **5**, there is only one Cu center called Cu1. For comparing the separation between K_1 and K_2 edges with axial bond lengths we have preferred to use only the distance Cu2-O for complex **2**. It can be seen from table 2 that for complexes **1**, **4**, **2**, **5** and **3** the separation between the K_1 and K_2 edges is 6.7, 6.6, 6.5, 6.5 and 6.1 eV respectively, while, the axial bond length is 2.47, 2.46, 2.45, 2.44 and 2.19 Å respectively, showing that the separation between the two edges decreases as the axial bond length Cu-O decreases, thereby implying that $4p_z$ destabilization has correlation with axial bond length.

3.3. Ab-initio XANES calculations

Ab-initio XANES calculations have been performed using the software *FEFF10* [32] to obtain simulated XANES spectra and also p and d-DOS for the complexes. The details of calculations are given in SI section S4.

The XANES spectra were simulated and the p- and d-DOS were calculated for the Cu1 centre in complex **1** and Cu2 centre in complex **2**. In complex **3**, there is only one Cu centre and the calculations were performed for that centre. The simulated spectra are given in figs. 6(a), (b), (c) and (d) for complexes **1**, **2**, **3** and **8** respectively. The experimental XANES spectra of the pertinent complexes are also included in these figures. The theoretical and experimental spectra shown in these figures are aligned by *Athena*. For complexes **4** and **5**, the fitting of experimental EXAFS data has been done using the theoretical model generated for complex **1** in section 3.1. Hence, the simulated XANES spectra and the theoretical p- and d-DOS obtained for complex **1** are assumed to be same for complexes **4** and **5**. Accordingly, the experimental XANES spectra for complexes **4** and **5** have also been included in fig. 6(a). For complex **6**, the fitting of experimental EXAFS data has been done using the theoretical model generated for complex **8**. Hence, the simulated XANES spectra and theoretical p- and d-DOS obtained for complex **8** are assumed to be same for complex **6**. Accordingly, the experimental XANES spectra for complex **6** have also been included in fig. 6(d). The features and shape of the experimental XANES spectra are reproduced quite well in the simulated XANES spectra. The theoretically calculated p-DOS, included in figs. 6(a-d) and d-DOS in fig. 7 have been further used for discussion given in the following sections.

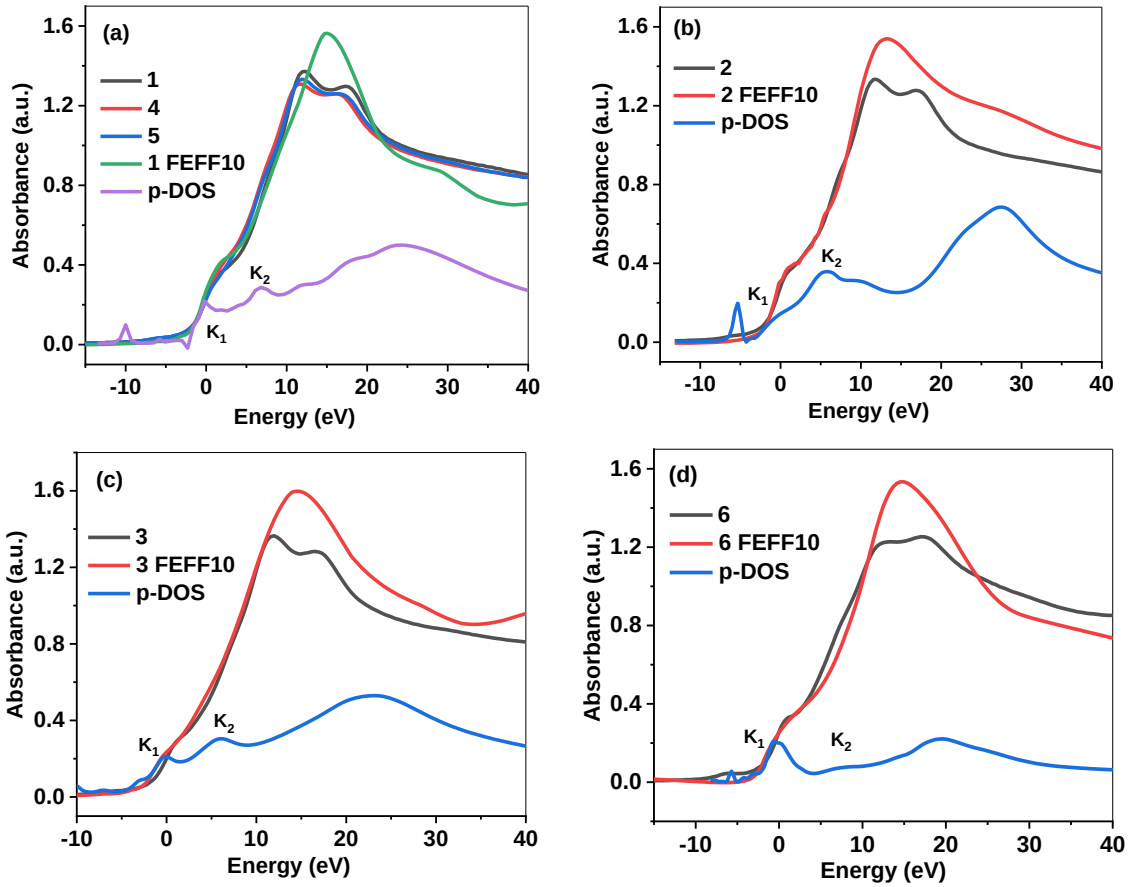

Fig.6 Simulated XANES spectra along with p-DOS for (a) complex **1**, (b) complex **2**, (c) complex **3**, (d) complex **8**. Experimental XANES spectra for (a) complexes **1**, **4** and **5** (b) complex **2** and (c) complex **3**, (d) complex **6**. The theoretical and experimental spectra have been aligned by *Athena*.

3.3.1. Correlation with the splitting of the edge: As already described in section 3.2.4, in all the six complexes, the Cu K-edge has been found to split into two edges K_1 and K_2, which arise due to the transitions $1s \rightarrow 4p_{xy}$ and $1s \rightarrow 4p_z$ respectively. We have attempted to explain the splitting of the K-edge on the basis of the theoretically calculated p-DOS shown in fig. 6(a-d). In the 4p density of states, there are two humps. The separation between the two humps in the complexes lies between the energy range 5-7 eV (table 2). This range of separation of the two humps in the p-DOS is nearly the same as the range of separation (6.1-6.7 eV) (table 2) between the experimental K_1 and K_2 edges of the complexes. The two humps in the p-DOS can thus be correlated with the two edges K_1 and K_2 and the splitting of the K-edge into K_1 and K_2 edges in the complexes can thus be understood on the basis of density of 4p states.

3.3.2. Correlation with pre-edge peak: As already described in section 3.2.2, the pre-edge peak P is observed as a weak feature on the lower energy side of the Cu K-edge in the

experimental XANES spectra of all the complexes (fig. 4(a) and 4(c)). The peak is attributed to the 1s→3d quadrupole transition [26]. The intensity of a transition is proportional to both the transition probability and the density of states [34,35]. The transition probability of 1s→3d transition which gives rise to this peak is very low, (of the order of <1/100) in comparison to the dipole transition 1s-4p which gives rise to the edge [26,35-37]. Hence, we have tried to correlate the occurrence of the peak to the 3d-density of states. The theoretical d-DOS have been computed for the complexes **1-3** and **8** using software *FEFF10* and are shown in fig. 7. For complexes **4** and **5**, the d-DOS can be taken to be similar to that for complex **1**. For complex **6**, it can be taken to be similar to that for complex **8**. In this figure, the peak value of the d-DOS has been observed in the energy range 10.4-15 eV below the position of the K-edge. For comparing the position of the pre-edge peak observed in the experimental spectra with the position of the peak in d-DOS, we have first determined the energy of the Cu K-edge in the complexes at μx=0.5 position in the experimental spectra of the complexes [30,31]. The position of centroid of the pre-edge peak in the experimental spectra is then found with respect to this Cu K-edge energy. The position of centroid thus calculated is given for all the complexes in table 3 and is found to be in the range 10.4-10.7 eV which is comparable to the position of the peak of the d-DOS which is in the range of 10.4-15 eV. Thus, the position of pre-edge peak in the experimental spectra corresponds to the position of the peak in theoretical d- density of states. The significant value of the density of d states, shown in fig. 7, is an important reason for the occurrence of pre-edge peak, though the quadrupole transition responsible for it has low probability.

3.3.3. Correlation with white line: In the experimental XANES spectra given in figs. 6(a-d), the white line is observed as a broadened structure having two peaks marked by two arrows as shown in the figures. However, in the simulated XANES spectra given in the same figures, the white line is observed as a single peak and the two-peak structure of the white line is not reproduced in the *FEFF10* calculations. Such difference in the experimental and the simulated XANES spectra has been discussed in detail by Chaboy et al. [38], who have shown that single-channel multiple-scattering calculations, taking the final state electronic configuration of Cu (II) as $3d^9$, are unable to reproduce the experimental two peak feature of a white line in Cu (II) complexes. Accordingly, they included in their calculations the contribution of two electronic configurations $3d^9$ and $3d^{10}L$ in the final state to account for a proper description of the final state during the photo absorption process. Good agreement

between theory and experiment was obtained by considering a relative weight of 68% and 32% for the two absorption channels $3d^{10}L$ and $3d^{9}$, respectively. The difference between the calculated binding energies for the two configurations was found to be 6.37 eV, while the experimental separation of the two peaks in the white line was 5.98 eV. In the present case, the experimental separation is 5.7-5.9 eV in complexes **1**-**5** and 5.0 eV in complex **6**. Hence, the splitting of the white line in complexes **1-6** can be attributed to the contribution of two electronic configurations $3d^{9}$ and $3d^{10}L$ in the final state during the photo absorption process.

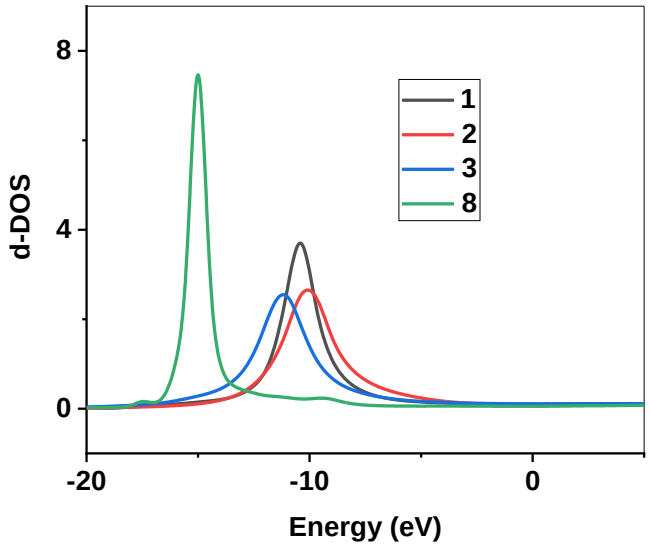

Fig.7 Theoretical d-DOS calculated by using FEFF10 for complexes **1-3** and **8**. For complexes **4** and **5**, it can be taken to be similar to that for complex **1**. For complex **6**, it can be taken to be similar to that for complex **8.**

4. Conclusions

XAFS at the Cu K-edge has been used to investigate the local coordination and electronic nature of Cu center in the copper benzimidazole mixed ligand complexes **1-6**. From EXAFS analysis, the geometry around Cu atom in complexes **1-5** has been estimated to be square pyramidal with four N atoms at distances 1.96-2.01 Å from the Cu atom forming the square base and the O atom at the top of pyramid at distance 2.19-2.55 Å from the Cu atom at the center of square base. The results for complexes **1** and **2** showed that information about the two Cu sites of the two independent formula units in a molecule can be obtained from EXAFS. By using three different theoretical models, the structure of complex **6** is suggested to be tetrahedrally distorted square planar around the central Cu

atom with the four N atoms having Cu atom at the center, the Cu-N distances being in the range from 1.93-1.99 Å.

XANES spectra simulated using the selected theoretical models from EXAFS fitting, show main edge features similar to those present in the experimental XANES spectra. Cu K-edge of the complexes is observed to split into two edges K_1 and K_2. In the 4p density of states, there are two humps having separation of 5-7 eV, which is nearly the same as the separation of 6.1-6.7 eV between the experimental K_1 and K_2 edges of the complexes. The two humps in the p-DOS can thus be correlated with the two edges K_1 and K_2 and the splitting of the K-edge into K_1 and K_2 edges in the complexes can thus be understood on the basis of density of 4p states.

The position of centroid of the pre-edge peak in the experimental spectra (10.4-10.7 eV) is found to correspond to the position of the peak in theoretical d- density of states (10.4-15 eV). The significant value of the density of d states is an important reason for the occurrence of pre-edge peak, though the quadrupole transition responsible for it has low probability. The white line in complexes **1-6** was observed to split into two peaks due to the contribution of two electronic configurations $3d^9$ and $3d^{10}L$ in the final state.

Acknowledgement

V.K. Hinge and M. Bairagi would like to thank the University Grant Commission-Department of Atomic Energy-Consortium for Scientific Research, Indore, for the research project grant No. CSR-IC-ISUM-24/CRS-307/2019-20/1359.

Supplementary material

Supplementary material associated with this article can be found, in the online version, at doi:

References

[1] L. Sieron, Tetrakis(1H-benzimidazole-kN^3)(sulfato-kO)- copper(II) dimethyl sulfoxide solvate, Acta Crystallogr. E 63 (2007) m579-580

[2] D. Dobrzynska, J. Janczak, A. Wojciechowska, K. Helios, Structure and spectroscopic study of a novel complex: Tetrakis(benzimidazole)(perchlorato)copper(II)(perchlorate) hemihydrate, J. Mol. Struct. 973 (1-3) (2010) 62–68

[3] F. Téllez, H. López-Sandoval, S.E. Castillo-Blum, and N. Barba-Behrens, Coordination behavior of benzimidazole, 2-substituted benzimidazoles and benzothiazoles, towards transition metal ions, Arkivoc, V (2008) 245-275

[4] S.B. Miao, B. M. Ji, and C. X. Du, Synthesis and crystal structure of two Cu(II) complexes with benzimidazole ligands, Russ. J. of Coord. Chem., 37(6) (2011) 468–472.

[5] B.M. Jia, S.B. Miao, D.S. Denga, C.X. Du, The C–H..Cl_2Cu(II) synthon in the structural direction and assembly of supramolecular complexes with the 3,3′-bis(2-benzimidazolyl)-2,2′-dipyridine ligand and its N-substituted derivatives, Polyhedron 28(13) (2009) 2611–2618

[6] S. B. Miao, B. M. Ji, D. S. Deng, C. Xu, and N. Ma, Crystal structures and luminescence of two Zinc(II) complexes with benzimidazole ligands, J. Struct. Chem., 51(2) (2010) 386-391

[7] S. Liu, J. Zuo, Y. Li, X. You, Syntheses, crystal structures of blue luminescent complexes based on 2,6-bis(benzimidazolyl) pyridine, J. Mol. Struc., 705(1-3) (2004) 153–157

[8] M. Bukowska-Strzyzewska and A. Tosik, Crystal and molecular structure of dibromobis(benzimidazole)copper(II): A low-temperature investigation, J. Crystallog. Spectros. Res., 21(3) (1991) 379-383

[9] M.S. Haddad and D.N. Hendrickson, Magnetic exchange interactions in binuclear transition-metal complexes. 15. copper(II) and nickel(II) complexes bridged by imidazolate, benzimidazolate, biimidazolate, and bibenzimidazolate ions, Inorg. Chem., 17(9) (1978) 2622-2630

[10] F.L. Zhou and S. Weng N, Tetrakis (1H-benzimidazole- κN^3) (nitrato-κO) copper (II) nitrate, Acta Cryst., E 67(6) (2011) m792

[11] M. Goodgame and L. I. B. Haines, Copper(II) complexes of benzimidazole, J. Chem. Soc. (A) (1966) 174-177

[12] M. Cordes and J. L. Walter, Infrared and Raman studies of heterocyclic compounds--H infrared spectra and normal vibrations of benzimidazole and bis-(benzmidazolato)-metal complexes, Spectrochimica Acta, 24A(9) (1968) 1421-1435

[13] R.J. Sundberg and R. Bruce Martin, Interactions of histidine and other imidazole derivatives with transition metal ions in chemical and biological systems, Chem. Rev., 74(4) (1974) 471-516

[14] D.P. Drolet, D.M. Manuta, A.J. Lees, FT-IR and XPS study of copper(I1) complexes of imidazole and benzimidazole, Inorganica Chim. Acta, 146(2) (1988) 173-180

[15] M. Good game and F. A. Cotton, Preparation and magnetic and spectral studies of some cobalt(II) complexes of benzimidazole, J. Amer. Chem. Soc., 84(9) (1962) 1543-1548

[16] V.K. Hinge, S.K. Joshi, B.D. Shrivastava, J. Prasad and K. Srivastava, X-ray absorption studies of copper (II) mixed ligand complexes with benzimidazole as one of the ligands, Indian J. Pure and Appl. Phys., 49(3) (2011) 168-172

[17] V.K. Hinge, S.K. Joshi, N.N. Nair, V.S. Verma, B.D. Shrivastava, J. Prasad and K. Srivastava, Extended X- ray absorption fine structure study at the K-edge of copper in mixed ligand complexes having benzimidazole as one of the ligands, J. Phys.: Conf. Ser. 534 (2014) 012024

[18] S. Dwivedi, S.K. Joshi, V.K. Hinge, B.D. Shrivastava, J. Prasad and K. Srivastava, XAFS study of benzimidazole mixed ligand complexes of copper, AIP Conf. Proc., 2100 (2019) 020194

[19] A. Gaur, D.Ah. Dar, B.D. Shrivastava, J. Prasad, K. Srivastava, S.N. Jha and D. Bhattacharyya, Performance of BL-8 dispersive and BL-9 scanning EXAFS beamlines at Indus-2 synchrotron, Indian J. Phys., 89(5) (2015) 453-462.

[20] B. Ravel, M. Newville, Athena, Artemis, Hephaestus: data analysis for X-ray absorption spectroscopy using IFEFFIT, J. Synchrotron Radiat., 12(4) (2005) 537-541

[21] J. Wang, C. Dai and D. Zhao, Bis[2-(1H-benzimidazol-2-yl)benzoato]- copper(II) dihydrate, Acta Cryst., E66(10) (2010) m1306–m1307

[22] P.M. Selvakumar, S. Nadella, K.J. Prathap, R.I. Kureshy, E. Suresh, P.S. Subramanian, Synthesis, crystal structure, and catalytic studies on dinuclear copper(II) mesocates, Inorganica Chim. Acta, 375(1) (2011) 106-113

[23] N. Kitajima, T. Katayama, K. Fujisawa, Y. Iwata and Y. Moro-oka, Synthesis, molecular structure, and reactivity of (Alkylperoxo)copper (II) complex, J. Am. Chem. Soc. 115(17) (1993) 7872-7813

[24] A. Gaur, W. Klysubun, Balram Soni, B.D. Shrivastava, J. Prasad, K. Srivastava, Identification of different coordination geometries by XAFS in copper(II) complexes with trimesic acid, J. Mol. Struc., 1121 (2016) 119-127.

[25] A. Gaur, B.D. Shrivastava, K. Srivastava and J. Prasad, XAFS study of aqua (diethylenetriamine)(isonicotinato)- copper (II) complex – inference of square pyramidal geometry, X-ray Spectrom., 43(4) (2014) 238-245.

[26] R.A. Bair and W.A. Goddard, Ab initio studies of the x-ray absorption edge in copper complexes. I. Atomic Cu^{2+} and Cu(II)Cl_2, Phys. Rev., B 22(6) (1980) 2767-2776

[27] S. Adak, M. Hartl, L. Daemen, E. Fohtung, H. Nakotte, Study of oxidation states of the transition metals in a series of Prussian blue analogs using x-ray absorption near edge structure (XANES) spectroscopy, J. Electron Spectros. Relat. Phenom., 214 (2017) 8–19

[28] F. de Groot, G. Vankó, P. Glatzel, The 1s X-ray absorption pre-edge structures in transition metal oxides. J. Phys. Condens. Matter**,** 21(10) (2009) 104207

[29] M. Newville, Larch: An analysis package for XAFS and related spectroscopies, J. Phys.: Conf. Ser., 430 (2013) 012007.

[30] C. Lamberti, S. Bordiga, F. Bonino, C. Prestipino, G. Berlier, L. Capello, F. D'Acapito, F. X. Llabre´s i Xamena and A. Zecchina, Determination of the oxidation and coordination state of copper on different Cu-based catalysts by XANES spectroscopy in situ or in operando conditions, Phys. Chem. Chem. Phys., 5(20) (2003) 4502–4509

[31] S. Calvin, XAFS for Everyone, CRC Press, Boca Raton, Florida, USA (2013) page 17

[32] J.J. Rehr, J.J. Kas, F.D. Vila, M.P. Prange, K. Jorissen, Parameter-free calculations of X-ray spectra with FEFF9, Phys. Chem. Phys. Chem., 12(21) (2010) 5503-5513

[33] J.J. Kas, F. D. Vila, and J. J. Rehr, C. D. Pemmaraju, T. S. Tan, Advanced calculations of x-ray spectroscopies with FEFF10 and Corvus, J. Synchrotron Radiat., 28(6) (2021) 1801-1810

[34] N. Sarmaha, D. Sharma, B.K. Mehta, B.D. Shrivastava, B.K. Das, A. Zimina, A. Gaur, Probing the electronic nature of Co centers forming the planar ring in octa-nuclear Co complexes using X-ray absorption spectroscopy, J. Mol. Struc. 1263 (2022) 133125.

[35] M. A. Blokhin, The Physics of X-rays, Second, Revised Edition, United States Atomic Energy Commission, Office of Technical Information, Germantown, Maryland, USA (1961), page 285.

[36] B.K. Agarwal, X-Ray Spectroscopy, Springer-Verlag, Berlin, Heidelberg, Germany (1989) page 92-94.

[37] J.H. Scofield, Relativistic Hartree-slater values for K and L X-ray emission rates, Atom. Data Nucl. Data Tables, 14(2) (1974) 121–137.

[38] J. Chaboy, A. Munoz-Paez, F. Carrera, P. Merkling, E.S. Marcos, Ab initio x-ray absorption study of copper K-edge XANES spectra in Cu(II) compounds, Phys. Rev., B 71(13) (2005) 134208

Supporting information

XAFS study of mixed ligand benzimidazole copper complexes having distorted coordination geometry

V.K. Hinge[a], M. Bairagi[a*], N. Yadav[b], B.D. Shrivastava[b], S.N. Jha[c], D. Bhattacharya[d] and A. Gaur[e*]

[a]Physics Department, Ujjain Engineering College, Ujjain, 456010, India

[b]School of Studies in Physics, Vikram University, Ujjain, 456010, India

[c]Beamline Development and Application Section BARC, Mumbai-400085 and BARC Beamlines Section, RRCAT, Indore, 452013, India

[d]Atomic & Molecular Physics Division, Bhabha Atomic Research Centre, Mumbai, 400085, India

[e]Institute for Chemical Technology and Polymer Chemistry (ITCP), Karlsruhe Institute of Technology, 76131 Karlsruhe, Germany

*monicabairagi14@gmail.com, *abhijeet.gaur@kit.edu

S1. List of complexes with their codes and molecular formula

Code	Name	Molecular formula
1	Cu (BzImH)$_4$ (ClO_4)$_2$	Cu[$C_6H_4N(NH)CH]_4(ClO_4)_2$
2	Cu (BzImH)$_4$ (NO_3)$_2$	Cu[$C_6H_4N(NH)CH]_4(NO_3)_2$
3	Cu (BzImH)$_4$ SO_4	Cu[$C_6H_4N(NH)CH]_4SO_4$
4	Cu (BzImH)$_4Br_2$	Cu[$C_6H_4N(NH)CH]_4Br_2$
5	Cu (BzImH)$_4$ Cl_2	Cu[$C_6H_4N(NH)CH]_4Cl_2$
6	Cu (BzIm)$_2$	Cu[$C_6H_4N(NH)CH]_2$
7	Cu [2-(1H-benzimidazol-2-yl) benzoato]$_2$ $2H_2O$	[Cu($C_{14}H_9N_2O_2)_2$] $2H_2O$
8	[$Cu_2(L_1)_2$].EtOH	$Cu_2C_{44}H_{42}N_4O_5$

Notes: BzIm=benzimidazole, L_1=m-xylenediamine

Complexes **1-6** have been investigated in the present work

The available crystallographic data of complexes **7** [21] and **8** [22] have been used for generating theoretical models

S2. Details of EXAFS analysis

The analysis of the experimental EXAFS of the complexes has been done by generating the theoretical models and fitting them to the experimental data using software *Artemis*. While performing the fittings, a single value of S_0^2 and ΔE_0 has been defined for all the paths, but different values of ΔR have been defined for different paths. Debye-Waller factor (σ^2) values have been defined for each type of scattering path. The input parameter R_{bkg} was set to 1 Å.

The k weight of 2 is used in all the cases. The ranges of the R-space and k-space in which these fittings have been done are different for each complex and are given below for the complexes.

Complex **1**: k range=2.5-11.8 $Å^{-1}$, R range=1-3.2 Å
Complex **2**: k range=2.5-12.5 $Å^{-1}$, R range=1-3.0 Å
Complex **3**: k range=2.4-12.2 $Å^{-1}$, R range=1-3.3 Å
Complex **4**: k range=2.4-11.6 $Å^{-1}$, R range=1-3.2 Å
Complex **5**: k range=2.5-10.5 $Å^{-1}$, R range=1-3.3 Å
Complex **6**: k range=2.6-11.8 $Å^{-1}$, R range=1-3.2 Å

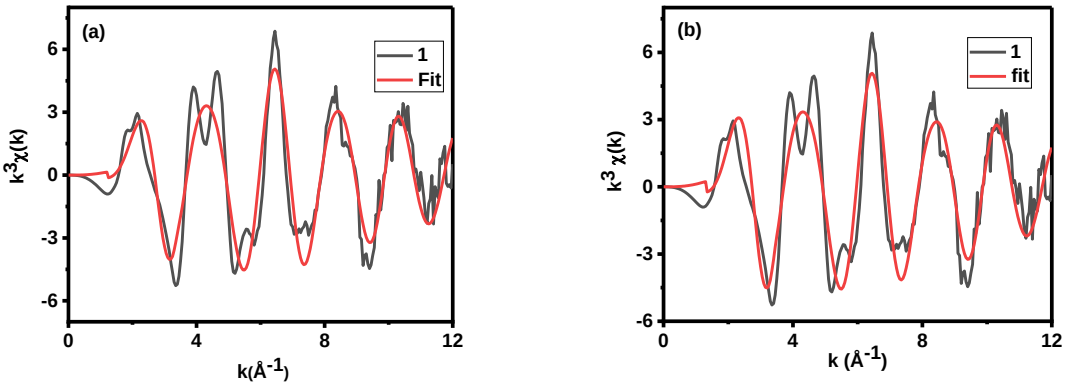

Fig.S1 EXAFS fitting for complex **1** in k-space, showing the experimental curve (black line) and the theoretical fit (red line) with the theoretical models generated using its own crystallographic data for (a) Cu1 site and (b) Cu2 site.

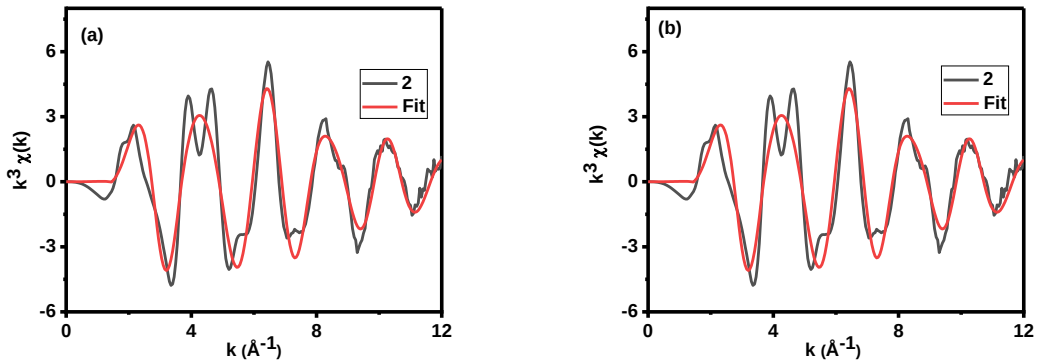

Fig. S2 EXAFS fitting for complex **2** in k-space, showing the experimental curve (black line) and the theoretical fit (red line) with the theoretical models generated using its own crystallographic data for (a) Cu1 site and (b) Cu2 site.

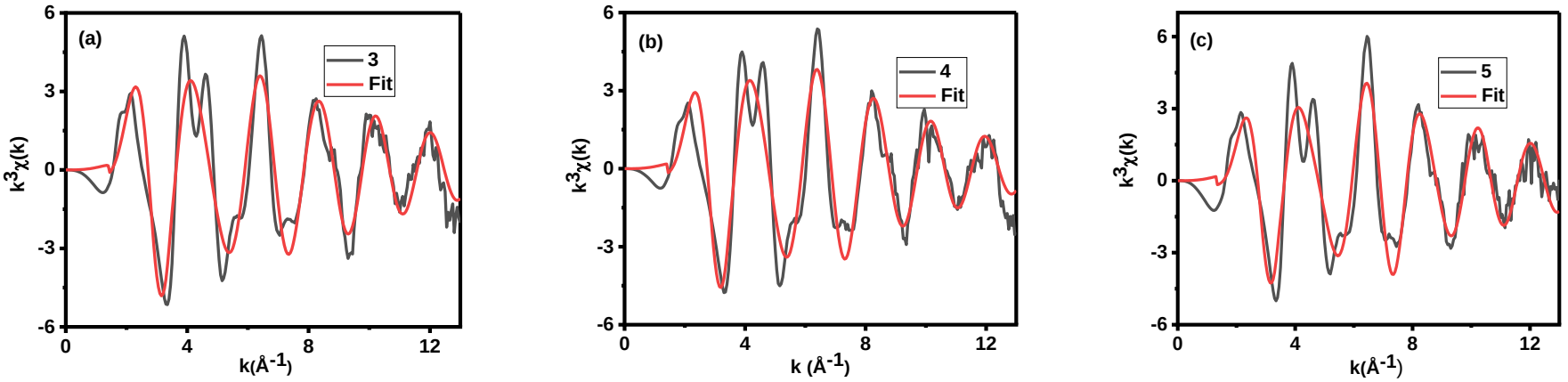

(a) (b) (c)

Fig. S3 EXAFS fitting in k-space, showing the experimental curve (black line) and the theoretical fit (red line).
(a) Complex **3.** Theoretical model generated using its own crystallographic data.
(b) Complex **4**. Theoretical model generated using crystallographic data of complex **1** (Cu1 site)
(c) Complex **5**. Theoretical model generated using crystallographic data of complex **1** (Cu1 site)

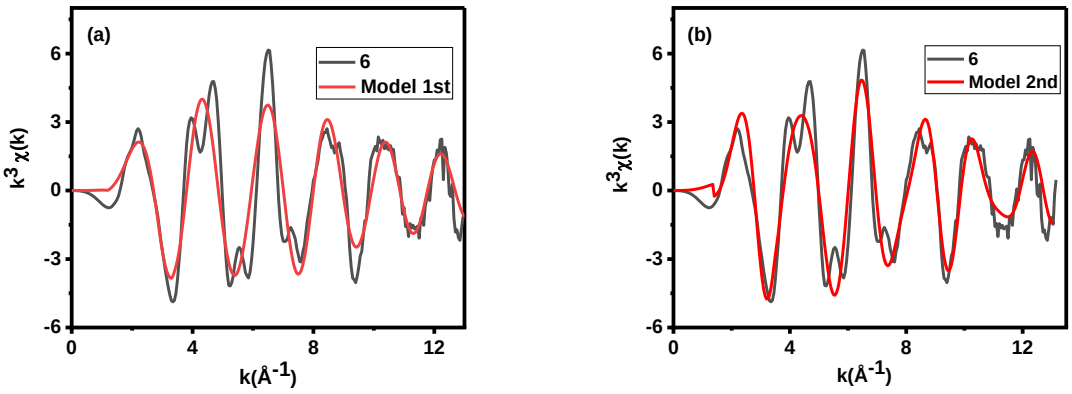

(a) (b)

Fig.S4 EXAFS fitting for complex **6** in k-space, showing the experimental curve (black line) and the theoretical fit (red line)

(a) Theoretical model generated using crystallographic data of complex **7** (square planar geometry).

(b) Theoretical model generated using crystallographic data of complex **8** (tetrahedrally distorted square planar geometry).

S3. Analysis of pre-edge peak using the module available in software *Larch* [29] and fitting it by Pseudo-Voigt function.

Fig. S5 (a-f) Pseudo-Voigt curve fitting of pre-edge peak for the complexes **1-6**.

(a) Complex **1** $[Cu(BzImH)_4](ClO_4)_2$

Centroid = 8977.8 eV, height =9.2×10^{-3}, area (amplitude) = 5.8×10^{-2} and reduced chi square (χ^2_ν) = 3.7×10^{-8}

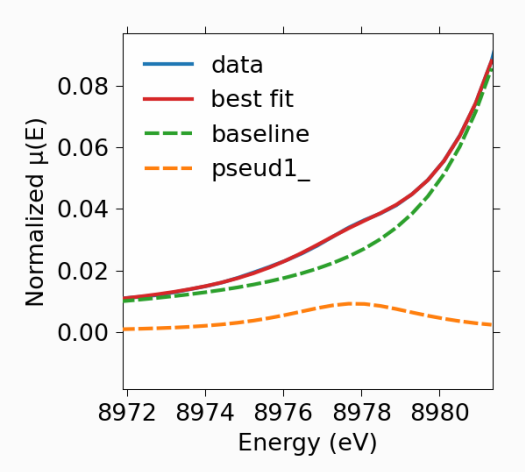

(b) Complex **2** $[Cu(BzImH)_4](NO_3)_2$.

Centroid = 8977.6 eV, height = 6.2×10^{-3}, area (amplitude) = 1.4×10^{-2} and

reduced chi square (χ_v^2) = 3.0×10^{-8}

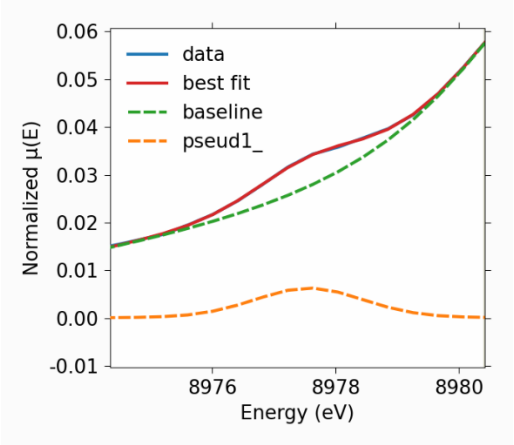

(c) Complex **3** $[Cu(BzImH)_4]SO_4$.
Centroid = 8977.6 eV, height = 4.4×10^{-3}, area (amplitude) = 1.1×10^{-2} and reduced chi square (χ_v^2) = 3.7×10^{-8}

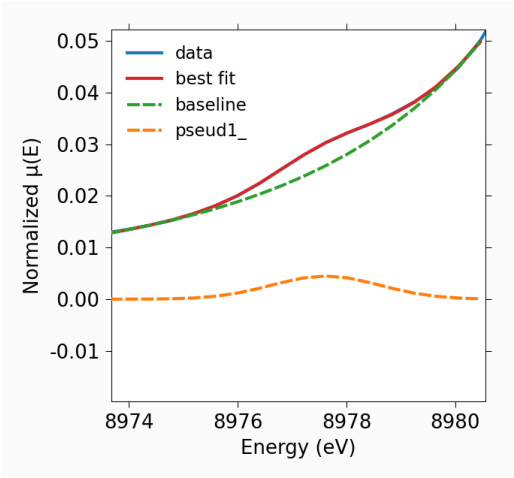

(d) Complex **4** $[Cu(BzImH)_4]Br_2$.
Centroid = 8977.1 eV, height = 6.4×10^{-3}, area (amplitude) = 2.7×10^{-2} and reduced chi square (χ_v^2) = 2.5×10^{-8}

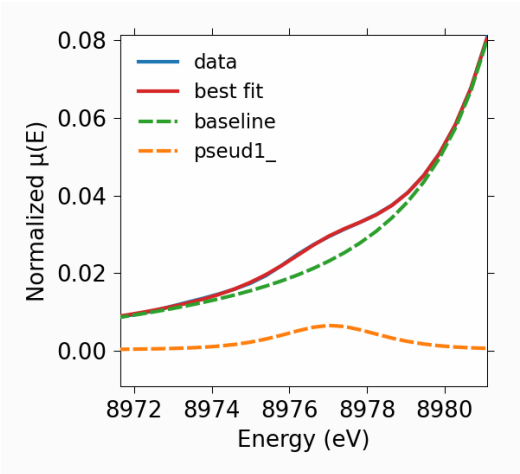

(e) Complex **5** $[Cu(BzImH)_4]Cl_2$.
Centroid = 8977.1 eV, height = 6.3×10^{-3}, area (amplitude) = 2.1×10^{-2} and

reduced chi square (χ_v^2) = 8.3×10^{-8}

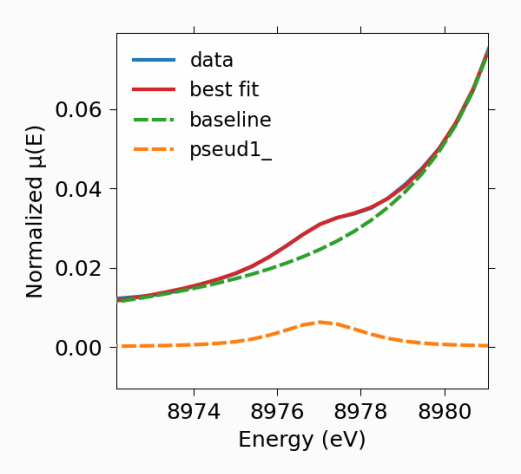

(f) Complex **6** $[Cu(BzImH)_2]$.
Centroid = 8976.7 eV, height = 13×10^{-3}, area (amplitude) = 3.5×10^{-2} and reduced chi square (χ_v^2) = 2.1×10^{-8}

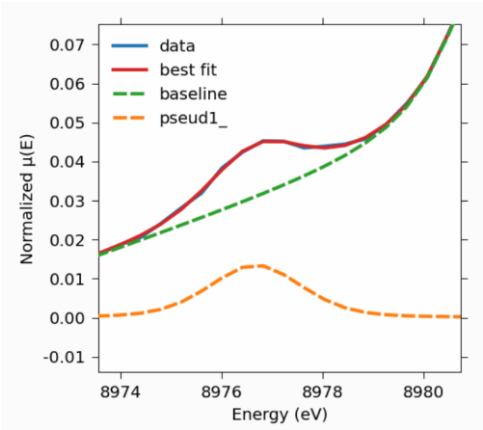

S4. Details of XANES calculations

Ab-initio XANES calculations have been performed using the software *FEFF10* [32] to obtain simulated XANES spectra and also p and d-DOS for the complexes. For the calculations, the input file feff.inp has been generated by utilizing the available crystal structure data [1, 2, 10, 22]. In the calculations, Hedin-Lundqvist potential was chosen and the cards called 'XANES', 'Exchange', 'SCF' (Self-Consistent Field) and 'FMS' (Full Multiple Scattering) were used [33]. The self-consistent potential (SCF) parameters were kept as follows: nscmt = 100, lfms1 = 0, rfms1 = 4, ca = 0.2, nmix = 1. The XANES parameters were as follows: vixan = 0.1, xkstep = 0.25, xkmax = 4. For density of states calculations, the 'LDOS' card with an energy range of −20 to 40 eV has been used.